HHS Public Access

Author manuscript

Exp Neurol. Author manuscript; available in PMC 2018 February 01.

Published in final edited form as:

Exp Neurol. 2017 February ; 288: 153–166. doi:10.1016/j.expneurol.2016.11.015.

Neurotoxic mechanisms of paclitaxel are local to the distal axon and independent of transport defects

Erica L. Gornstein[1,2] and **Thomas L. Schwarz**[1]

[1]The F.M. Kirby Neurobiology Center, Children's Hospital Boston, Boston, MA 02115, USA

[2]Biological and Biomedical Sciences Program, Harvard Medical School, Boston, MA 02115, USA

Abstract

Chemotherapy-induced peripheral neuropathy (CIPN) is a dose-limiting side effect of paclitaxel and other chemotherapeutic agents. Paclitaxel binds and stabilizes microtubules, but the cellular mechanisms that underlie paclitaxel's neurotoxic effects are not well understood. We therefore used primary cultures of adult murine dorsal root ganglion neurons, the cell type affected in patients, to examine leading hypotheses to explain paclitaxel neurotoxicity. We address the role of microtubule hyperstabilization and its downstream effects. Paclitaxel administered at 10–50 nM for 1–3 days induced retraction bulbs at the tips of axons and arrested axon growth without triggering axon fragmentation or cell death. By correlating the toxic effects and microtubule stabilizing activity of structurally different microtubule stabilizing compounds, we confirmed that microtubule hyperstabilization, rather than an off-target effect, is the likely primary cause of paclitaxel neurotoxicity. We examined potential downstream consequences of microtubule hyperstabilization and found that changes in levels of tubulin posttranslational modifications, although present after paclitaxel exposure, are not implicated in the paclitaxel neurotoxicity we observed in the cultures. Additionally, defects in axonal transport were not implicated as an early, causative mechanism of paclitaxel's toxic effects on dorsal root ganglion neurons. By using microfluidic chambers to selectively treat different parts of the axon with paclitaxel, we found that the distal axon was primarily vulnerable to paclitaxel, indicating that paclitaxel acts directly on the distal axon to induce degenerative effects. Together, our findings point to local effects of microtubule hyperstabilization on the distal-most portion of the axon as an early mediator of paclitaxel neurotoxicity. Because sensory neurons have a unique and ongoing requirement for distal growth in order to reinnervate the epidermis as it turns over, we propose that the ability of paclitaxel to arrest their growth accounts for the selective vulnerability of sensory neurons to paclitaxel neurotoxicity.

Keywords

paclitaxel; Taxol; chemotherapy-induced peripheral neuropathy; neurotoxicity; microtubule; sensory neuron

Corresponding Author: Thomas L. Schwarz, Thomas.schwarz@childrens.harvard.edu, F.M. Kirby Neurobiology Center, Center for Life Sciences, Rm. 12-130, 3 Blackfan Circle, Boston, MA 02115.

Introduction

Paclitaxel is a widely used chemotherapeutic that frequently causes peripheral neuropathy. The neuropathy, which can be dose-limiting, primarily affects sensory neurons and leads to a distal axonopathy; patients with paclitaxel-induced peripheral neuropathy experience loss of sensation and ongoing pain in the hands and feet and demonstrate degeneration of the nerve fibers that innervate the skin (1). Paclitaxel binds to the interior of microtubules and stabilizes them, interfering with the normal cycling of microtubule depolymerization and repolymerization. In dividing cells such as cancer cells, this disrupts normal spindle dynamics, interferes with mitosis, and ultimately leads to cell death (2). Neurons, which do not divide, are nevertheless susceptible to paclitaxel, and the mechanisms underlying paclitaxel neurotoxicity remain incompletely elucidated (reviewed in (3)). Developing interventions for paclitaxel-induced peripheral neuropathy will require understanding the mechanisms by which paclitaxel compromises peripheral axons.

Axons are rich in microtubules, which provide structural support and serve as tracks for axonal transport throughout the life of the neuron. While neurons have a larger population of stable microtubules than non-neuronal cells, their microtubules are not static. Given paclitaxel's action in dividing cells, it has been presumed that increased microtubule stabilization contributes to paclitaxel neurotoxicity. However, alternative binding targets leading to effects on the ER and mitochondria have been proposed that may be relevant (4–6). Determining whether microtubule stabilization is the primary cause of paclitaxel neurotoxicity is a first step in defining the mechanistic pathways leading to neuronal damage.

If microtubule stabilization is the primary cause of paclitaxel neurotoxicity, the cellular mechanisms that link microtubule hyperstabilization and axon degeneration are unknown. One known consequence of increased microtubule stabilization is a change in the levels of tubulin posttranslational modifications, namely increased acetylation, polyglutamylation and detyrosination (7–9). Tubulin post-translational modifications can alter the binding of microtubule-associated proteins and motors, and alterations in these modifications have been linked to axon degeneration and regeneration. For example, tyrosinated tubulin is necessary for the binding of microtubule plus-end interacting proteins that are required for transport initiation at the distal axon (10, 11). Tubulin hyperglutamylation has been linked to Purkinje cell degeneration and increases the activity of the microtubule severing protein, spastin (12, 13). Additionally, microtubule deacetylation is required for axon regeneration after injury (14), and kinesin-1 based transport is affected by acetylation and detyrosination (15–19). Thus it is plausible that the alterations in tubulin post-translational modifications observed in neurons upon paclitaxel treatment contribute to paclitaxel neurotoxicity, a hypothesis which has not yet been tested.

A prevalent hypothesis for how microtubule stabilization could ultimately lead to axon degeneration is through the disruption of axonal transport. Previous studies have observed paclitaxel-induced defects in axonal transport. These studies, however, mostly employed cell types other than the clinically affected mammalian sensory neuron (20–22), or used paclitaxel concentrations higher than the peak plasma concentrations typically reached in

patients (23, 24). The relevance of potential transport defects as an early, causative event in paclitaxel neurotoxicity is uncertain.

Using cultured adult mammalian dorsal root ganglion (DRG) neurons, we examined the role of microtubule stabilization and its downstream consequences in paclitaxel neurotoxicity. Our results suggest that increased microtubule stabilization, rather than an off-target effect, is likely to be responsible for paclitaxel neurotoxicity. However, our results do not point to an early causative role of changes in tubulin post-translational modifications or axonal transport defects in paclitaxel's toxic effect on axons, but indicate instead a direct vulnerability to paclitaxel of the distal-most portion of the axon. Inhibiting growth at the distal axon may account for the sensory neuropathy.

Results

Modeling paclitaxel neurotoxicity in cultured adult DRG neurons

In order to interrogate mechanisms of paclitaxel neurotoxicity, we established a model of paclitaxel-induced degeneration in cultured adult mammalian DRG neurons, the neuron type relevant to the clinical problem of paclitaxel-induced peripheral neuropathy. The use of cultures necessarily restricted the study to cell autonomous aspects of the neuropathology although other cell types are also likely to contribute (25, 26). For probing mechanisms of paclitaxel neurotoxicity, we thought it important to use paclitaxel concentrations that resulted in a slow time course of degeneration in order to untangle whether potential mechanisms were a likely primary cause rather than indirect consequence of degeneration. To this end, we used dissociated cultures of DRGs from 8–10 week old mice and exposed them to nanomolar concentrations of paclitaxel that led to degenerative effects over the course of days. Treatment of these sensory neuron cultures with 10–50 nM paclitaxel led within three days to a dose-dependent increase in bulbous swellings mostly at the axon tips, an appearance consistent with retraction bulbs (Fig 1A–B). Axon area relative to untreated cultures decreased with a similar time course (Fig 1C). After one day in 10 nM paclitaxel, there were scattered bulbous axon swellings, which were more frequent upon exposure to 25 or 50nM paclitaxel. At each concentration, their frequency was further increased relative to control after three days of paclitaxel exposure (Fig 1B). After three days in 25 nM or 50 nM paclitaxel, axon area per field was also decreased, axon width was increased, and axons appeared abnormally wavy. Nonetheless, the number of cell bodies per imaging field did not change compared to control, indicating that in these treatment conditions, paclitaxel was toxic to axons but did not cause cell death (Fig 1D). Because low nanomolar concentrations of paclitaxel led to a slow time course of quantifiable degenerative effects, we used this concentration range to probe paclitaxel neurotoxicity mechanisms. Peak plasma concentrations after common dosing regimens in patients are in the range of 228 nM-4.3 uM (27), but the concentrations experienced by the neurons are not known. The range of 10–50 nM therefore seemed appropriate for dissociated DRG neurons in culture that likely have better access and less transient exposure to the drug than neurons in vivo.

We characterized further the retraction bulb-like swellings that formed after paclitaxel exposure. Unlike the growth cones of control axons, the retraction bulbs did not have actin extending beyond the microtubules (Fig 1E). Microtubule polymerization was disordered in

the retraction bulbs as evidenced by swirling EB3-GFP comets (Movie S1, Movie S2). Additionally, while the level of acetylated tubulin overall increased after paclitaxel treatment, indicative of stable microtubules, tubulin in retraction bulbs was predominantly deacetylated (Fig 1F). Furthermore, retraction bulbs had accumulations of mitochondria (Fig 1G). These observations are consistent with descriptions of CNS retraction bulbs, which are characterized by disorganized microtubules (28).

We wondered whether neuronal types differed in their response to paclitaxel in vitro and therefore whether neuronal type may be an important consideration when selecting a model for mechanistic studies of paclitaxel neurotoxicity. We found that different neuron types had different sensitivities and morphological responses to paclitaxel. In particular, cultured hippocampal neurons were more sensitive than DRG neurons to paclitaxel when both were exposed to 50 nM paclitaxel for three days. Microtubules were fragmented in hippocampal neurons and their axons were no longer intact (Fig 1H). This fragmentation was not observed in DRG cultures, even after three days in 1 μM paclitaxel (data not shown). Prior to fragmentation, hippocampal neurons did have some axonal swellings that might be akin to the retraction bulbs of DRG neurons. After one day of 50 nM paclitaxel treatment, bulbous structures were observed in hippocampal neurons near the soma at the tips of very short neurites (data not shown); this response to paclitaxel has been previously reported at higher concentrations in younger embryonic cortical neuron cultures (29). Previous work on younger hippocampal cultures has shown that microtubule stabilization causes neurons to form multiple axons when far lower doses of paclitaxel (3 nM) are applied (30). Adult DRG axons are thicker, more robust, and more tubulin-rich than embryonic hippocampal neurons and thus the different responses of the neurons to 50 nM paclitaxel may reflect either age-dependent (31) or cell-type specific differences. The axonal effects seen in adult DRG neurons after paclitaxel treatment better resemble the “dying back” axon retraction characteristic of paclitaxel-induced peripheral neurotoxicity (1) and thus may be preferable to hippocampal neurons for mechanistic studies.

The neurotoxicity of epothilone B and paclitaxel correlates with their microtubule stabilization

As a first step in defining mechanistic pathways that lead to paclitaxel neurotoxicity, we tested the hypothesis that increased microtubule stability, rather than off-target effects, is the primary cause of paclitaxel neurotoxicity. Although a change in microtubule dynamics after paclitaxel exposure has been a dominant hypothesis to explain paclitaxel neurotoxicity, alternative paclitaxel binding targets have been described: neuronal calcium sensor-1 and the apoptosis regulator Bcl-2 (4–6). To test this hypothesis, we examined epothilone B, a microtubule stabilizing compound that binds to a site on tubulin that overlaps the taxane site but is structurally different from paclitaxel; epothilone B would therefore be unlikely to have the same off-target effects (32). If microtubule overstabilization is responsible for paclitaxel neurotoxicity, it is expected that the prodegenerative capacity of paclitaxel and epothilone B will correlate with the degree of microtubule stabilization. We examined microtubule stability in cultured adult DRG neurons biochemically by assessing relative levels of soluble βIII tubulin after treatment with 2 nM paclitaxel or epothilone B, replenishing the compounds every 8 hours to maintain steady concentrations. 2 nM epothilone B strongly

increased microtubule stability, as evidenced by a marked decrease in soluble βIII tubulin comparable to what is seen with 25 nM paclitaxel, but 2 nM paclitaxel was much less effective (Fig 2A). This difference in potency at 2 nM allowed us to compare the prodegenerative effects of the compounds. 2 nM epothilone B, which substantially stabilized microtubules already at 24 hours, also significantly induced the incidence of retraction bulbs, though 2 nM paclitaxel did not. After 72 hours, 2 nM epothilone B was also significantly more potent in causing retraction bulbs (Fig 2B–C). In addition, 2 nM epothilone B decreased axon area compared to control, while paclitaxel did not (Fig 2D–E). While the axon area decreased after epothilone B treatment, the number of cell bodies per field did not change, suggesting that, as with 25 nM paclitaxel, epothilone causes axonal toxicity rather than cell death (Fig 2F). Overall, the morphological effects of epothilone B and paclitaxel on DRG neurons were very similar, but epothilone B was roughly an order of magnitude more potent than paclitaxel both in microtubule stabilizing activity and degenerative effects; neurons treated with 2 nM epothilone B resembled neurons treated with 25 nM paclitaxel. This correlation of microtubule stabilization and prodegenerative effects for structurally dissimilar compounds supports the hypothesis that increased microtubule stability, rather than an off-target effect, is responsible for paclitaxel neurotoxicity.

Changes in levels of tubulin modification do not correlate with retraction bulb formation

Why might increased microtubule stability be toxic to neurons? Stable microtubules have increased levels of tubulin acetylation, polyglutamylation and detyrosination. These tubulin post-translational modifications have been implicated in regulating axonal transport (15–19), binding of microtubule-related proteins (11, 12), and neuron health (13, 14). We therefore tested the hypothesis that changes in tubulin post-translational modifications contribute to paclitaxel neurotoxicity as reflected in the formation of retraction bulbs; to this end, we manipulated the level or activity of the enzymes that control the cycling of tubulin modifications.

Treatment of cultured DRG neurons with 25 nM paclitaxel led to an increase in glutamylated tubulin as determined by immunocytochemistry and Western blot (Fig 3A–C). By expressing shRNA against TTLL1, the catalytic subunit of the neuronal polyglutamylase, control levels of glutamylated tubulin could be maintained even after paclitaxel treatment (Fig 3A–C). Despite this rescue of glutamylation levels, the induction of retraction bulbs after paclitaxel treatment was not ameliorated (Fig 3D–E). These data suggest that increased tubulin glutamylation is not required for paclitaxel neurotoxicity.

25 nM paclitaxel also increased levels of acetylated tubulin in DRG axons (Fig 4A–B). To determine whether this increase contributed to paclitaxel-induced toxicity, we asked whether increasing the acetylation of tubulin mimics paclitaxel induction of retraction bulbs. Neurons were treated with the HDAC6 inhibitor tubacin to prevent deacetylation and thereby increase tubulin acetylation to similar levels as caused by paclitaxel (Fig 4A–B). The paclitaxel and tubacin increases in tubulin acetylation were also apparent in axons permeablized with triton prior to fixation to extract soluble tubulin, indicating that the acetylated tubulin was incorporated into microtubules (data not shown). Unlike paclitaxel, tubacin did not cause retraction bulbs after either one or three days exposure (Fig 4C–D). That increased levels of

acetylated tubulin were not sufficient to mimic paclitaxel's effects on DRG axons suggests that the increase of acetylated tubulin is not a major contributor to paclitaxel neurotoxicity.

Stable microtubules have high ratios of detyrosinated to tyrosinated tubulin and DRG axons treated with 50 nM paclitaxel have correspondingly decreased tyrosinated tubulin levels (Fig 5A–B). To ask if this decrease contributes to paclitaxel neurotoxicity, the tyrosinating enzyme, tubulin tyrosine ligase (TTL) was overexpressed which caused control axonal levels of tyrosinated tubulin to be maintained after paclitaxel exposure (Fig 5A–B). The tyrosinated tubulin was resistant to triton permeabilization and therefore incorporated into microtubules (data not shown). Despite preventing the paclitaxel-induced decrease in tyrosinated tubulin, TTL expression did not prevent the formation of retraction bulbs (Fig 5C). Thus changes in tubulin tyrosination are not required for paclitaxel neurotoxicity. Together, our manipulations of tubulin post-translational modifications indicate that although tubulin modifications are altered by paclitaxel treatment, they are unlikely to be responsible for the early paclitaxel-induced signs of neurodegeneration.

Effects of paclitaxel exposure on axonal transport of mitochondria and late endosomes/lysosomes in cultured adult DRG neurons

A prevalent hypothesis to link microtubule stabilization and axon degeneration invokes defects in axonal transport (33–35). We therefore asked whether axonal transport defects arise in adult sensory neurons prior to overt fragmentation of axons and might thus be a cause rather than consequence of neurotoxicity. To that end, 25 nM paclitaxel was applied to adult DRG neurons, a condition in which axons remained intact but nonetheless developed scattered retraction bulbs after one day and, after three days, had broader axons with more retraction bulbs and more sparsely covered the field.

Mitochondria are of particular interest to paclitaxel-induced neuropathy because swollen and functionally deficient mitochondria have been observed in the peripheral nerves of animal models (36, 37), and mitochondrial transport defects are implicated in several neurodegenerative disorders (38). Mitochondria were therefore labeled with Mito-dsRed via lentiviral transduction and their movements in a mid-axonal segment were imaged one and three days after 25 nM paclitaxel treatment (Fig 6A–B). The percent time that mitochondria spent in retrograde motion was slightly increased after one day of paclitaxel (Fig 6C), however after three days of paclitaxel treatment there was no difference compared to vehicle control in either anterograde or retrograde movement (Fig 6E). We did observe some changes in mitochondrial velocities; retrograde speed was increased at both one and three days of paclitaxel exposure, while anterograde speed was decreased, though only after one day of paclitaxel treatment (Fig 6D, F). Peak plasma concentrations of paclitaxel in typical dosing regimens are in the range of 230 nM-4.3 μM (27). We therefore tested 250 nM and 2.5 μM paclitaxel for effects on mitochondrial transport after 6–9 hr of paclitaxel exposure, after microtubules would be stabilized but prior to visible signs of neurotoxicity. Although small changes in the parameters of movement were noted, they did not follow a clear dose-response relationship (Fig 6G–J). For example, anterograde mitochondrial motility decreased slightly and retrograde speed increased slightly with 250 nM paclitaxel, but these differences were not observed with exposure to 2.5 μM paclitaxel (Fig 6G–J). Thus,

although we looked over a broad range of concentrations and time points, paclitaxel's effects on mitochondrial transport were modest and did not correlate well with the observed toxicity; these data point away from a primary defect of mitochondrial transport as a cause of paclitaxel neurotoxicity.

We also examined the effect of paclitaxel on transport of late endosomes and lysosomes by expressing LAMP1-RFP. Because of the large number of fast-moving RFP-positive particles in the axon, we analyzed organelle flux rather than the tracks of individual organelles. While there was no difference in either anterograde or retrograde flux after one day of 25 nM paclitaxel treatment, retrograde flux of lysosomes along the axon slightly decreased after three days of paclitaxel treatment (Fig 7A–D). The observed changes in late endosomes and lysosomes thus do not parallel the modest changes seen in mitochondrial transport; whereas retrograde mitochondrial transport increased after one day of paclitaxel, retrograde flux decreased for late endosomes/lysosomes after longer paclitaxel exposure.

Exposure of the distal, but not the mid-axon, to paclitaxel disrupts axon outgrowth

Because paclitaxel treatment decreased axon area of cultured adult DRG neurons, we examined the effects of paclitaxel on axon outgrowth by repeat imaging of GFP-expressing neurons that had been cultured for six days and then exposed to 50 nM paclitaxel. Grooves were scored into the culture substrate with a pin rake and dissociated neurons were plated as a spot so that axons would extend in an orderly fashion between the grooves. This allowed us to evaluate the growth of multiple axons in a single imaging field. At 2.5, 14 or 38 hours after paclitaxel addition, a given field was imaged at 20 minute intervals for 100–120 minutes to evaluate the position of identified tips of axons. After just 2.5 hours of 50 nM paclitaxel treatment, axon extension was reduced to 9.2% of vehicle treated control (Fig 8A, D). This nearly complete arrest of axon outgrowth was also apparent 14 and 38 hours after paclitaxel addition (Fig 8B–C); many individual axons had no outgrowth or retracted their axons during the 100–120 minutes of imaging. These results are consistent with the previous finding that a higher concentration of paclitaxel, 700 nM, arrests outgrowth of one day old chick sensory neurons in culture (39).

We used this assay to examine further the relevance of axonal transport defects to paclitaxel-induced peripheral neuropathy and employed microfluidic devices to isolate paclitaxel exposure to either mid-axons or distal axons. Dissociated DRG neurons were plated into the somal compartment and axons grew through microgrooves into a 500 μm mid-axon compartment and then through a second set of microgrooves into a 1500 μm distal compartment (Fig 9A). Though the mid-axon compartment was smaller than the distal, the axons were much less straight in the mid-axon channel, and therefore it is likely that comparable lengths of axon were exposed to paclitaxel when it was added to either compartment. Trypan blue was used in pilot studies to confirm that fluidic isolation was maintained over the course of the experiment. Mid or distal axons of adult DRG neurons were selectively treated with 50 nM paclitaxel for two days after which multiple fields in the distal compartment were imaged every 20 minutes for 120 minutes, as in Fig 8. The addition of paclitaxel to the distal axon compartment decreased growth of distal axons; many axons did not grow or retracted during the imaging period. In contrast, when the mid-axons were

exposed to paclitaxel, the growth of the distal axons was not significantly different from control (Fig 9B). This result indicates that the distal axon in particular is vulnerable to paclitaxel, and suggests that local effects of paclitaxel in the distal axon play a role in paclitaxel neurotoxicity. Because growth cone dynamics depend on selective stabilization and retraction of pioneer microtubules (40), the indiscriminate stabilization of microtubules in the growth cone may be sufficient to explain the arrest of growth we observe.

Discussion

By using cultured DRG neurons to investigate paclitaxel-effects on axons, we could control the level of paclitaxel exposure, limit it to restricted regions of the axon, monitor in detail axonal transport, and manipulate biochemical pathways previously implicated in the toxicity of chemotherapeutics. Although a murine model may imperfectly reflect events in human neurons, we approximated the most clinically relevant population of cells by using DRG neurons from adult mice. We found that equivalent doses of paclitaxel had quite different effects on E18 hippocampal neurons than on adult DRGs. Previous studies in cultures and in vivo have gained significant insight into the mechanism of paclitaxel with systems as diverse as Drosophila, Aplysia, and zebrafish, and with rodent neuronal populations from embryonic DRG and hippocampi (3, 22, 25, 41, 42). By selecting cultured neurons for their advantages in imaging and biochemical manipulations, we have necessarily restricted ourselves to cell autonomous mechanisms and forgone the ability to examine the effects of paclitaxel on other cell types that may contribute to neuropathy, including inflammatory responses and effects on Schwann cells or epithelial targets (25, 26).

One difficulty in probing neurotoxic mechanisms has been distinguishing early, causative effects from later consequences of neurodegeneration. We therefore used concentrations of paclitaxel that led to neurotoxic effects on DRG neurons, but did not cause rapid axon fragmentation or cell death. Patients do not experience dramatic destruction of all sensory axons, as can occur in response to very high concentrations of paclitaxel in other cell types, but rather lose a portion of the sensory endings and usually after repeated paclitaxel exposures (1). The changes in axons that we observed may therefore be similar to early events that occur in patients. Although the concentrations used in this study are below reported maximum plasma doses in patients (27), axons within the complex environment of peripheral nerves are unlikely to experience the peak plasma concentration and those concentrations are not sustained.

In DRG neurons exposed to paclitaxel, axon outgrowth stopped and bulbous endings known as retraction bulbs formed. These endings contained dynamic, disorganized and deacetylated microtubules and accumulations of mitochondria and presumably other organelles. We therefore used axon density and the frequency of retraction bulbs as a proxy for the dying back neurodegenerative effect of paclitaxel in vivo.

Microtubule hyperstabilization is the best studied cellular action of paclitaxel and is often, but not always (4, 35), presumed to underlie its neurotoxicity. We therefore compared the efficacies of epothilone B and paclitaxel, two structurally unrelated stabilizers of microtubules that likely would have different off-target effects. The degree of microtubule

stabilization induced by these compounds correlated well with their prodegenerative capacity in cultured DRG neurons. Consistent with our observation of epothilone B as a more potent microtubule stabilizer than paclitaxel, epothilone is generally more toxic than paclitaxel to cancer cell lines (32). Moreover, treatment with ixabepilone, an analog of epothilone B, also leads to a sensory peripheral neuropathy in patients (43). Our results indicate that excess microtubule stabilization is likely to be the primary effect of paclitaxel that initiates the downstream neurotoxic events. The WldS mouse and calpain inhibition offer some protection against paclitaxel-induced degeneration (44, 45), and NMNAT overexpression protects against the degeneration in a fly model (41); these interventions likely block the downstream degeneration pathway triggered by microtubule stabilization.

What are the cellular mechanisms by which increased microtubule stabilization is neurotoxic? We explored two current hypotheses: that changes in tubulin post-translational modifications (46) or disruption of axonal transport are responsible for the degeneration. Though we confirmed that paclitaxel changes tubulin modifications in DRG neurons, the changes in acetylation, glutamylation or tyrosination appeared unrelated to retraction bulb formation. Manipulations that either mimicked the hyperacetylation, or prevented the increase in glutamylated or decrease in tyrosinated tubulin did not mimic or prevent the formation of retraction bulbs. Although there remains the possibility that a combination of several of these changes would have uncovered an effect that our individual manipulations did not, there was no noticeable decrease in the retraction bulb phenotype when tubulin glutamylation and tyrosination changes were prevented. These posttranslational modifications appear unlikely to cause the neurotoxicity in this system.

The length of sensory axons may make them highly dependent on microtubule-based transport of organelles, proteins and mRNA. The vital role of axonal transport is underscored by mutations in motor proteins and defects in transport that are associated with neurodegenerative diseases (47). We therefore looked closely at the effects of paclitaxel on mitochondrial transport but did not observe any consistent defect in mitochondrial transport; though minor changes in individual parameters were sometimes observed, none correlated with either dose or duration and thus did not appear related to growth arrest or retraction bulb formation. In neurodegenerative diseases that take decades to develop such as Alzheimer’s disease, Amyotrophic Lateral Sclerosis, or Huntington’s disease, transport perturbations too subtle to be detected by our assays might over time lead to axonal degeneration. In this study, however, paclitaxel arrested axonal growth within 2.5 hours and produced retraction bulbs within one to three days, and undetectable changes in transport are therefore an unlikely cause.

Previous studies of paclitaxel have observed bulk axonal transport defects at high paclitaxel concentrations (10 uM and 200 uM, higher than the maximum plasma concentration reported in patients) (23, 24). Studies using lower paclitaxel concentrations have also observed bulk transport decreases (21, 22, 48) and mitochondrial transport decreases (20, 49), however these studies were not carried out on adult mammalian DRG neurons.

Selectively exposing either mid or distal axons to paclitaxel provided an independent approach to interrogate a causative role of potential transport defects along the axon to

paclitaxel neurotoxicity without presupposing which trafficked cargo would be most critical. We reasoned that a defect due to axonal transport should, given sufficient time of exposure, manifest itself whether the block was close to the axon tip or in the middle of the axon. We found that even two days of exposure of the medial portion of axon to paclitaxel did not impede the growth of axons although comparable exposure of the distal axon did. These findings again point away from axonal transport defects as an early event in paclitaxel neurotoxicity.

A previous study in cultured neurons found that paclitaxel directly acts on peripheral sensory axons rather than the soma: when embryonic DRG neurons were grown in microfluidic devices such that paclitaxel could be selectively added to the axons or cell bodies, axon length was reduced specifically when the axons were treated with paclitaxel (42). Our study has taken the next step by comparing regions of the axon and has shown that the distal portion of the axon is selectively sensitive. In contrast to the lack of an effect when paclitaxel was applied for two days but prevented from contacting the distal portion, arrest of growth followed within 2.5 hours of exposure when the entire axon was exposed. The results of the present study parallel those of Silva et al. (50), who found that, specifically at low dose, the microtubule destabilizing agent vincristine was toxic when added to the distal, but not the mid-axon, suggesting that a selective vulnerability of the distal axon could be a commonality for microtubule-targeting agents. Furthermore, study of a low-dose rodent model of paclitaxel-induced peripheral neuropathy found that degeneration was limited to the sensory fibers innervating the epidermis and supports the particular sensitivity of these distal nerve endings to paclitaxel (51).

Recent studies of growth cone dynamics have determined that microtubules play a key role in both axon elongation and growth cone guidance (52, 53). Filipodial extension is driven by actin treadmilling, but microtubule growth and retraction, particularly for pioneer microtubules, are also required for growth cone motility and consequently undergo extensive regulation (40). Thus it is likely that indiscriminate stabilization of microtubules in growth cones *per se* is sufficient to prevent axon elongation and induce retraction bulbs without further changes in tubulin modifications or microtubule-based transport. In injured spinal cord neurons, however, low doses of paclitaxel have been shown to enhance axon regrowth and prevent retraction bulbs from forming (28, 54). In the context of injury when a glial scar is forming and microtubules are destabilized, low doses of paclitaxel may restore correct microtubule dynamics and axon extension. Thus the consequences of paclitaxel may be very context dependent.

The selective vulnerability of the distal axon to paclitaxel in cultured neurons may arise from changes to microtubule dynamics in the growth cone and raises the question of whether this is a phenomenon of relevance to mature sensory neurons in vivo that are not in a comparable state of regeneration. Nerve fiber endings that innervate the skin are not, however, static. It is estimated that the epidermis completely turns over in 40–56 days, and in response nerve endings likely periodically remodel by withdrawing and then repenetrating the layers of keratinocytes of the epidermis (51, 55, 56). GAP-43, a marker of axon growth and plasticity, is present in a subset of nerve fibers in the dermis and epidermis in skin of the adult hand (57). Thus sensory neurons may be dependent on axon extension and local

microtubule dynamics in vivo as well as in culture. Furthermore, a recent GWAS study has found an association in patients between genes involved in axon outgrowth and the severity of paclitaxel-induced peripheral neuropathy (58). Maintenance of appropriate contact of nerve fibers with the skin is important for continued retrograde survival signals at the distal axon that play a role in maintaining axonal health (59). Thus, paclitaxel's negative effect on the plasticity of the distal axon suggests a hypothesis in which the inability to remodel in response to the changing microenvironment of the epidermis in vivo could eventually lead to neurite retraction and degeneration and may be an initial insult in paclitaxel-induced degeneration. Furthermore, secondary to a neurite remodeling defect and retraction, disruption of cellular processes at the distal axon, such as autophagosome formation (60) and endocytosis of survival factors (59) could contribute to the pathogenesis.

One of the outstanding questions for chemotherapy-induced peripheral neuropathy has been the selective vulnerability of sensory neurons over motor neurons. One current hypothesis is that the cell bodies of sensory neurons lie outside the blood brain barrier and are therefore exposed to higher levels of the chemotherapeutic than those of motor neurons within the spinal cord. Because we find that the distal axon is the site of paclitaxel action in cultured sensory neurons, this hypothesis appears unlikely. Instead, we speculate that the difference in vulnerability arises from the ongoing remodeling at adult sensory endings, which contrasts with the stability of neuromuscular junctions. The initiating event is likely to be the stabilization of microtubules in the growth cones of those sensory endings that need to advance and reinnervate the epidermis during the administration of the drug. Because microtubule stabilization is the mode of action for both the therapeutic and neurotoxic actions of paclitaxel and related compounds, strategies to alleviate the neurotoxicity may need to focus on downstream pro-degenerative events.

Materials and Methods

Neuron culture

Dorsal root ganglia (DRG) from 8–10 week old male C57Bl/6J mice (Jackson labs) were dissected into cold HBSS (Life Technologies) containing 1% penicillin-streptomycin (Life Technologies) and dissociated in 1 mg/mL Collagenase A + 2.4 U/mL dispase II (Roche) for 70 min at 37°C, followed by 5 min in 0.25% trypsin (Life Technologies) at 37°C. After addition of trypsin inhibitor (Sigma) and washes, DRG were triturated using glass pasteur pipettes of decreasing size in the presence of 125U DNAse I (Sigma) and centrifuged through 10% BSA (Sigma). The cell pellet was washed and then resuspended in Neurobasal A (Life Technologies) with 2% B27 (Life Technologies), 100 U/mL penicillin-streptomycin, 1 mM L-glutamine (Life Technologies), 100 ng/μl NGF (Life Technologies), and 2 ng/μl GDNF (Sigma). 12–18 × 10^3 neurons/well were plated on acid washed glass coverslips (Bellco Glass) in a 24-well plate that had been coated overnight with 100 μg/ml poly-d-lysine (Sigma) at room temperature and 10 μg/ml laminin (Life Technologies) for 2 hr at 37°C. Beginning on DIV 1, 10 μM AraC (Sigma) was added to media.

Hippocampal neurons were isolated from embryonic day 18 rats (Charles River) as previously described (61), and plated at 8 × 10^4/well in a 24-well plate on acid washed coverslips that had been coated overnight at room temperature with 20 μg/ml poly-L-

ornithine (Sigma) and 3.5 μg/ml laminin. Cells were cultured in Neurobasal with 2% B27, supplemented with L-glutamine and penicillin-streptomycin.

Spot-Groove Culture

To grow straight axons for live imaging of distal axon endings, an optical-quality 24-well plate (Ibidi) was coated with poly-d-lysine and laminin as described above for DRG neuron culture. After coating, grooves were etched into each well using a pin rake (Tyler Research). DRG from 8–10 week old male mice were dissected and dissociated as described above and spotted in the center of the grooves at 15×10^3 cells/well in 7 μl of media. After allowing cells to attach for 1 hr in the incubator, media (Neurobasal A, 2% B27, 100 U/mL penicillin-streptomycin, 1 mM L-glutamine, 100 ng/μl NGF, 2 ng/μl GDNF) was slowly added. Beginning on DIV 1, 10 μM AraC was added to media. For live imaging of distal axons, cultures were infected with GFP-ires-GFP lentivirus at DIV 0, and cultures were grown for 6 DIV before treatment with paclitaxel.

Microfluidic devices

Acid washed coverslips (Warner Instruments 24×50 mm) were coated with 100 μg/ml poly-d-lysine overnight at room temperature. After washes with ddH_2O, TCND500 microfluidic devices (Xona Microfluidics) were attached to coverslips, and laminin was added to the channels at a concentration of 10 μg/ml for 3 hr at 37°C. DRG from 8–10 week old male mice were dissected and dissociated as described above and plated at 8×10^4 cells/microfluidic device in 5 μl of media. After allowing cells to attach for 55 min in the incubator, media (Neurobasal A, 2% B27, 100 U/mL penicillin-streptomycin, 1 mM L-glutamine, 50 ng/μl NGF, 1 ng/μl GDNF) was added slowly to the cell body wells. A portion of the cells in each device washed away when media was added. Media with 100 ng/μl NGF and 2 ng/μl GDNF was added to the axonal wells. Starting on DIV 1, 10 μM AraC was added to media. Media was changed every 2 days until DIV 6, when axons were treated with paclitaxel. Paclitaxel-containing media was replenished after 1 day.

Constructs and Compounds

The following lentiviral constructs were used in this study: EB3-GFP (62), and TTLL1-specific shRNA and control vector (Rogowski et al., 2010). TTL-ires-GFP, which was generated by cloning the coding sequence of human TTL from cDNA (GenBank BC036819) into pHAGE-CMV-ires-GFP (63). GFP-ires-GFP was used as a control plasmid. Mito-dsRed-ires-GFP, which was generated by cloning Mito-dsRed (Clontech) into pHAGE-CMV-ires-GFP. LAMP1-RFP-2A-GFP, which was generated by cloning LAMP1-RFP (Addgene #1817) into pLenti-CMV-2A-GFP (gift from C. Woolf).

Paclitaxel (Sigma), (−)-Epothilone B (Sigma) and Tubacin (Enzo Life Sciences) were kept as stocks in DMSO and were diluted in culture medium immediately prior to addition to cells. Control cultures always received an equivalent amount of DMSO.

Lentivirus preparation

Lentiviral particles were produced by cotransfection of lentiviral expression vectors with packaging helper plasmids into HEK293T cells plated in 15 cm^2 dishes. Media containing

viral particles was collected 48 and 72 hr after transfection. After filtration through a 0.45 μm filter, lentiviral particles were concentrated by spinning at 25,900 RPM at 4°C for 90 min (SW 32 Ti rotor, Beckman Coulter). The resulting viral pellet was resuspended in PBS/0.001% Pluronic F68 (Sigma), concentrating 800-fold from the packaging cell media, and stored at −80°C until use. Lentivirus was added to 250 μL culture media 3–4 hr after plating, and media was changed 16–18 hr later. Expression of fluorescent protein in the neuron cell body was used to monitor lentivirus expression.

Immunoflourescence

DRG neurons were fixed in 4% paraformaldehyde in PBS for 15 min, permeabilized with 0.1% triton-X in PBS for 10 min, and blocked in 15% goat serum/1% BSA/0.1% triton-X in PBS. Primary and secondary antibodies were diluted in block and incubated for 1 hr each at room temperature. The following primary antibodies were used: mouse anti-βIII tubulin (1:800, Sigma), rabbit anti-TUJ1 (1:1000; Covance), chicken anti-GFP (1:500; Aves Labs), mouse anti-glutamylated tubulin GT335 (1:3000; AdipoGen), mouse anti-acetylated tubulin 6-11B-1 (1:1000; Sigma), rat anti-tyrosinated tubulin YL1/2 (1:1000; Abcam), rabbit-anti Tom20 (1:500; Santa Cruz Biotechnology). The following secondary antibodies were used at 1:500: AlexaFluor-488 anti-mouse, anti-rabbit, or anti-chicken, AlexaFluor-568 anti-rabbit, AlexaFluor-647 anti-mouse (Invitrogen), Cy3-conjugated anti-mouse, Cy5-conjugated anti-rat (Jackson ImmunoResearch). Images of fixed cells were acquired on a Nikon Eclipse E800, or when fluorescence was to be quantified, a Zeiss LSM 710 confocal microscope.

Soluble tubulin and actin extraction assay

Dissociated DRG were cultured directly on poly-d-lysine and laminin coated 24-well plates. After a wash with warm PBS, soluble protein was extracted by adding 100 μl microtubule stabilizing buffer (80 mM PIPES pH 6.8, 1 mM $MgCl_2$, 1 mM EGTA, 5% glycerol, 0.5% triton-X) containing 1 mM PMSF and protease inhibitor cocktail (Calbiochem) at 1:500 for 2 min at 37°C. Samples were centrifuged at 13,000 *g* for 10 min at 4°C, the supernatants were collected and Laemmli buffer was added to 1x. An equal volume of each sample was run for Western blot analysis.

Western blotting

Protein lysates were separated by 8% SDS-PAGE and blotted with the following primary antibodies: rabbit anti-TUJ1 (1:2500; Covance), mouse anti-β-actin AC-74 (1:5000; Sigma), mouse anti-glutamylated tubulin GT335 (1:2000; AdipoGen). HRP-conjugated secondary antibodies (1:5000; Jackson ImmunoResearch) and SuperSignal West Dura (Thermo Scientific) were used for chemiluminescent detection.

For assessing levels of glutamylated tubulin in DRG cultures, cells grown directly on poly-d-lysine and laminin coated 24-well plates were lysed in 1X Laemmli sample buffer and an equal volume of each sample was loaded onto the SDS-PAGE gel.

Live cell time lapse imaging acquisition and quantification

For live cell imaging of transport of mitochondria or late endosomes/lysosomes in DRG neurons, coverslips were transferred to petri dishes containing Hibernate A (BrainBits), with

2% B27 and 2 mM Glutamax (Life Technologies). DMSO or paclitaxel was added to the imaging media at the same concentration as was present in the growth media. Time lapse movies were acquired on a Zeiss LSM 710 confocal microscope using a 63×/N.A.0.90 water IR-Achroplan objective. Cells were maintained at 37°C on a temperature-controlled stage (PeCon, GmbH). For imaging of mitochondria and late endosomes/lysosomes, portions of axon 100 μm long were selected and traced at least 500 μm away from the cell body using the GFP signal. Mitochondria were imaged at 1 frame/1.58 sec for 5 min, and late endosomes/lysosomes for 3 min. EB3-GFP was imaged at 1 frame/3.9 sec for 3 min. Live imaging of mitochondria and late endosomes/lysosomes was performed on DIV 4 and 6, and imaging of EB3-GFP was performed on DIV 4.

The mitochondrial movement parameters “percent time in motion per axon” and “average speed per mitochondrion” were quantified in ImageJ. Kymographs were generated from time lapse movies after running the Image Stabilizer plugin when necessary and mitochondria tracks were analyzed by manual tracing using a custom macro, Kymolyzer, as previously described (64). The percentage of time mitochondria were in anterograde or retrograde motion per axon was calculated by averaging the percent of frames in a trace for which each mitochondrion moved (ranging from 0–100%) in a kymograph. An average speed for each mitochondrion was calculated as the average of all instantaneous speeds in a trace that were not zero. The overall average was then calculated using the data from each mitochondrion. Movement slower than 0.05μm/sec was considered zero.

To determine lysosome flux, a vertical line was drawn near the center of the generated kymograph, and the number of tracks crossing the line in the anterograde and retrograde direction were counted.

For live imaging of axon growth in spot-groove cultures, DIV 6 DRG neurons were treated with paclitaxel or DMSO vehicle in phenol red-free complete growth media. Images of axon endings expressing GFP were acquired using the 40× objective on a Nikon Eclipse Ti microscope with an environmental chamber. Axon fields for imaging were selected prior to paclitaxel treatment, and the same axon fields were imaged 2.5, 14 and 38 hr after paclitaxel treatment for 100–120 min, with an image captured every 20 min. Axon tips analyzed for growth were selected prior to visualizing the movies, and a line was drawn using ImageJ at the point reached by the axon tip at t=0 for each imaging session. The distance of the axon tip from this line was measured at each 20 min interval of the 100–120 min imaging period.

For live imaging of axon growth in microfluidic chambers, DIC images of axons in the distal channel were acquired using a 40× objective on a Nikon Eclipse Ti microscope with an environmental chamber. Multiple fields containing axonal endings were imaged repeatedly every 20 min for 120 min. Distal axon growth was analyzed as described above for spot-groove cultures.

Image analysis

To quantify changes in levels of modified tubulin by immunofluorescence, maximum intensity projections were created of images taken with a 63× objective using identical imaging settings. To limit quantification of fluorescence to neuronal cells and to remove

background, using ImageJ, the Huang threshold was applied to the βIII tubulin staining, and the mean intensity of acetylated, glutamylated, tyrosinated, or βIII tubulin within the thresholded βIII tubulin outline was calculated. The intensity from modified tubulin was divided by the βIII tubulin intensity for each condition. The average value from 3–4 imaging fields for each condition from each experiment was used for statistical analysis.

The number of retraction bulb-like swellings and the number of cell bodies per field was counted manually from images taken with a 10× or 20× objective using the Cell Counter plugin in ImageJ.

Neurite area per field was quantified with ImageJ from images taken with a 20× objective using a macro based on Pani et al. (65) for assessing neurite area in dense cultures with both dim and bright neurites. In summary, after background subtraction, contrast enhancement, and application of a Gaussian blur filter, cell bodies were deleted manually from the image. Next, edges were enhanced using the FeatureJ Laplacian plugin. After contrast enhancement and application of the Moments threshold, a mask was created, and the analyze particles function (size: 50-infinity) was used to determine the area of the axon. For axon area and retraction bulb quantification, 4–6 imaging fields per coverslip and 2 coverslips from each condition were quantified per experiment, and the average value from each experiment was used for statistical analysis.

Statistics

Data are expressed as mean ± SEM. Statistical analysis was performed using GraphPad Prism 6. The unpaired Student's t test or the Mann-Whitney U test was used assess the statistical significance of differences between conditions. For multiple comparisons, data were analyzed by two-way ANOVA with Bonferroni correction or Dunnett's post test. $p<0.05$ was considered significant.

Supplementary Material

Refer to Web version on PubMed Central for supplementary material.

Acknowledgments

This work was supported by National Institutes of Health R01GM069808 (T.L. Schwarz) and F31 NS089152 (E.L. Gornstein), and the Mather's Foundation (T.L. Schwarz).

The authors thank C. Janke, M. Verhage, C. Woolf, and M. Sahin for constructs; T. Omura, C. Su, and M. Costigan for technical advice on DRG cultures; S. Vasquez, K. Apaydin, and L. Mkhitaryan for assistance with hippocampal neuron cultures; and the CHB IDDRC Imaging Core (grant P30 HD18655).

References

1. Boyette-Davis JA, et al. Persistent chemoneuropathy in patients receiving the plant alkaloids paclitaxel and vincristine. Cancer Chemother Pharmacol. 2013; 71(3):619–626. [PubMed: 23228992]
2. Weaver BA. How Taxol/paclitaxel kills cancer cells. Mol Biol Cell. 2014; 25(18):2677–2681. [PubMed: 25213191]
3. Gornstein E, Schwarz TL. The paradox of paclitaxel neurotoxicity: Mechanisms and unanswered questions. Neuropharmacology. 2014; 76(Pt A):175–183. [PubMed: 23978385]

4. Boehmerle W, et al. Paclitaxel induces calcium oscillations via an inositol 1,4,5-trisphosphate receptor and neuronal calcium sensor 1-dependent mechanism. Proc Natl Acad Sci U S A. 2006; 103(48):18356–18361. [PubMed: 17114292]

5. Ferlini C, et al. Paclitaxel directly binds to Bcl-2 and functionally mimics activity of Nur77. Cancer Res. 2009; 69(17):6906–6914. [PubMed: 19671798]

6. Rodi DJ, et al. Screening of a library of phage-displayed peptides identifies human bcl-2 as a taxol-binding protein. J Mol Biol. 1999; 285(1):197–203. [PubMed: 9878399]

7. Hammond JW, et al. Posttranslational modifications of tubulin and the polarized transport of kinesin-1 in neurons. Mol Biol Cell. 2010; 21(4):572–583. [PubMed: 20032309]

8. Mansfield SG, Gordon-Weeks PR. Dynamic post-translational modification of tubulin in rat cerebral cortical neurons extending neurites in culture: effects of taxol. J Neurocytol. 1991; 20(8):654–666. [PubMed: 1682422]

9. Garnham CP, Roll-Mecak A. The chemical complexity of cellular microtubules: tubulin post-translational modification enzymes and their roles in tuning microtubule functions. Cytoskeleton (Hoboken). 2012; 69(7):442–463. [PubMed: 22422711]

10. Moughamian AJ, Osborn GE, Lazarus JE, Maday S, Holzbaur EL. Ordered recruitment of dynactin to the microtubule plus-end is required for efficient initiation of retrograde axonal transport. J Neurosci. 2013; 33(32):13190–13203. [PubMed: 23926272]

11. Peris L, et al. Tubulin tyrosination is a major factor affecting the recruitment of CAP-Gly proteins at microtubule plus ends. J Cell Biol. 2006; 174(6):839–849. [PubMed: 16954346]

12. Lacroix B, et al. Tubulin polyglutamylation stimulates spastin-mediated microtubule severing. J Cell Biol. 2010; 189(6):945–954. [PubMed: 20530212]

13. Rogowski K, et al. A family of protein-deglutamylating enzymes associated with neurodegeneration. Cell. 2010; 143(4):564–578. [PubMed: 21074048]

14. Cho Y, Cavalli V. HDAC5 is a novel injury-regulated tubulin deacetylase controlling axon regeneration. Embo j. 2012; 31(14):3063–3078. [PubMed: 22692128]

15. Cai D, McEwen DP, Martens JR, Meyhofer E, Verhey KJ. Single molecule imaging reveals differences in microtubule track selection between Kinesin motors. PLoS Biol. 2009; 7(10):e1000216. [PubMed: 19823565]

16. Dompierre JP, et al. Histone deacetylase 6 inhibition compensates for the transport deficit in Huntington's disease by increasing tubulin acetylation. J Neurosci. 2007; 27(13):3571–3583. [PubMed: 17392473]

17. Dunn S, et al. Differential trafficking of Kif5c on tyrosinated and detyrosinated microtubules in live cells. J Cell Sci. 2008; 121(Pt 7):1085–1095. [PubMed: 18334549]

18. Konishi Y, Setou M. Tubulin tyrosination navigates the kinesin-1 motor domain to axons. Nat Neurosci. 2009; 12(5):559–567. [PubMed: 19377471]

19. Maas C, et al. Synaptic activation modifies microtubules underlying transport of postsynaptic cargo. Proc Natl Acad Sci U S A. 2009; 106(21):8731–8736. [PubMed: 19439658]

20. Das V, Sim DA, Miller JH. Effect of taxoid and nontaxoid site microtubule-stabilizing agents on axonal transport of mitochondria in untransfected and ECFP-htau40-transfected rat cortical neurons in culture. J Neurosci Res. 2014; 92(9):1155–1166. [PubMed: 24788108]

21. LaPointe NE, et al. Effects of eribulin, vincristine, paclitaxel and ixabepilone on fast axonal transport and kinesin-1 driven microtubule gliding: implications for chemotherapy-induced peripheral neuropathy. Neurotoxicology. 2013; 37:231–239. [PubMed: 23711742]

22. Shemesh OA, Spira ME. Paclitaxel induces axonal microtubules polar reconfiguration and impaired organelle transport: implications for the pathogenesis of paclitaxel-induced polyneuropathy. Acta Neuropathol. 2010; 119(2):235–248. [PubMed: 19727778]

23. Nakata T, Yorifuji H. Morphological evidence of the inhibitory effect of taxol on the fast axonal transport. Neurosci Res. 1999; 35(2):113–122. [PubMed: 10616915]

24. Theiss C, Meller K. Taxol impairs anterograde axonal transport of microinjected horseradish peroxidase in dorsal root ganglia neurons in vitro. Cell Tissue Res. 2000; 299(2):213–224. [PubMed: 10741462]

25. Lisse TS, et al. Paclitaxel-induced epithelial damage and ectopic MMP-13 expression promotes neurotoxicity in zebrafish. Proc Natl Acad Sci U S A. 2016

26. Zhang H, et al. Dorsal root ganglion infiltration by macrophages contributes to paclitaxel chemotherapy induced peripheral neuropathy. J Pain. 2016
27. Huizing MT, et al. Pharmacokinetics of paclitaxel and metabolites in a randomized comparative study in platinum-pretreated ovarian cancer patients. J Clin Oncol. 1993; 11(11):2127–2135. [PubMed: 7901342]
28. Erturk A, Hellal F, Enes J, Bradke F. Disorganized microtubules underlie the formation of retraction bulbs and the failure of axonal regeneration. J Neurosci. 2007; 27(34):9169–9180. [PubMed: 17715353]
29. Chuckowree JA, Vickers JC. Cytoskeletal and morphological alterations underlying axonal sprouting after localized transection of cortical neuron axons in vitro. J Neurosci. 2003; 23(9): 3715–3725. [PubMed: 12736342]
30. Witte H, Neukirchen D, Bradke F. Microtubule stabilization specifies initial neuronal polarization. J Cell Biol. 2008; 180(3):619–632. [PubMed: 18268107]
31. Kole AJ, Annis RP, Deshmukh M. Mature neurons: equipped for survival. Cell Death Dis. 2013; 4:e689. [PubMed: 23807218]
32. Goodin S, Kane MP, Rubin EH. Epothilones: mechanism of action and biologic activity. J Clin Oncol. 2004; 22(10):2015–2025. [PubMed: 15143095]
33. Argyriou AA, Bruna J, Marmiroli P, Cavaletti G. Chemotherapy-induced peripheral neurotoxicity (CIPN): an update. Crit Rev Oncol Hematol. 2012; 82(1):51–77. [PubMed: 21908200]
34. Lee JJ, Swain SM. Peripheral neuropathy induced by microtubule-stabilizing agents. J Clin Oncol. 2006; 24(10):1633–1642. [PubMed: 16575015]
35. Miltenburg NC, Boogerd W. Chemotherapy-induced neuropathy: A comprehensive survey. Cancer Treat Rev. 2014; 40(7):872–882. [PubMed: 24830939]
36. Flatters SJ, Bennett GJ. Studies of peripheral sensory nerves in paclitaxel-induced painful peripheral neuropathy: evidence for mitochondrial dysfunction. Pain. 2006; 122(3):245–257. [PubMed: 16530964]
37. Zheng H, Xiao WH, Bennett GJ. Functional deficits in peripheral nerve mitochondria in rats with paclitaxel- and oxaliplatin-evoked painful peripheral neuropathy. Exp Neurol. 2011; 232(2):154–161. [PubMed: 21907196]
38. Sheng ZH, Cai Q. Mitochondrial transport in neurons: impact on synaptic homeostasis and neurodegeneration. Nat Rev Neurosci. 2012; 13(2):77–93. [PubMed: 22218207]
39. Letourneau PC, Ressler AH. Inhibition of neurite initiation and growth by taxol. J Cell Biol. 1984; 98(4):1355–1362. [PubMed: 6143759]
40. Bearce EA, Erdogan B, Lowery LA. TIPsy tour guides: how microtubule plus-end tracking proteins (+TIPs) facilitate axon guidance. Front Cell Neurosci. 2015; 9:241. [PubMed: 26175669]
41. Bhattacharya MR, et al. A model of toxic neuropathy in Drosophila reveals a role for MORN4 in promoting axonal degeneration. J Neurosci. 2012; 32(15):5054–5061. [PubMed: 22496551]
42. Yang IH, Siddique R, Hosmane S, Thakor N, Hoke A. Compartmentalized microfluidic culture platform to study mechanism of paclitaxel-induced axonal degeneration. Exp Neurol. 2009; 218(1):124–128. [PubMed: 19409381]
43. Ebenezer GJ, et al. Ixabepilone-induced mitochondria and sensory axon loss in breast cancer patients. Ann Clin Transl Neurol. 2014; 1(9):639–649. [PubMed: 25493278]
44. Wang MS, Davis AA, Culver DG, Glass JD. WldS mice are resistant to paclitaxel (taxol) neuropathy. Ann Neurol. 2002; 52(4):442–447. [PubMed: 12325073]
45. Wang MS, et al. Calpain inhibition protects against Taxol-induced sensory neuropathy. Brain. 2004; 127(Pt 3):671–679. [PubMed: 14761904]
46. Baas PW, Ahmad FJ. Beyond taxol: microtubule-based treatment of disease and injury of the nervous system. Brain. 2013; 136(Pt 10):2937–2951. [PubMed: 23811322]
47. Chevalier-Larsen E, Holzbaur EL. Axonal transport and neurodegenerative disease. Biochim Biophys Acta. 2006; 1762(11–12):1094–1108. [PubMed: 16730956]
48. Goshima Y, Hida T, Gotoh T. Computational analysis of axonal transport: a novel assessment of neurotoxicity, neuronal development and functions. Int J Mol Sci. 2012; 13(3):3414–3430. [PubMed: 22489159]

49. Bober BG, Gutierrez E, Plaxe S, Groisman A, Shah SB. Combinatorial influences of paclitaxel and strain on axonal transport. Exp Neurol. 2015; 271:358–367. [PubMed: 26143110]
50. Silva A, Wang Q, Wang M, Ravula SK, Glass JD. Evidence for direct axonal toxicity in vincristine neuropathy. J Peripher Nerv Syst. 2006; 11(3):211–216. [PubMed: 16930282]
51. Bennett GJ, Liu GK, Xiao WH, Jin HW, Siau C. Terminal arbor degeneration--a novel lesion produced by the antineoplastic agent paclitaxel. Eur J Neurosci. 2011; 33(9):1667–1676. [PubMed: 21395870]
52. Buck KB, Zheng JQ. Growth cone turning induced by direct local modification of microtubule dynamics. J Neurosci. 2002; 22(21):9358–9367. [PubMed: 12417661]
53. Stout A, D'Amico S, Enzenbacher T, Ebbert P, Lowery LA. Using plusTipTracker software to measure microtubule dynamics in Xenopus laevis growth cones. J Vis Exp. 2014; (91):e52138. [PubMed: 25225829]
54. Hellal F, et al. Microtubule stabilization reduces scarring and causes axon regeneration after spinal cord injury. Science. 2011; 331(6019):928–931. [PubMed: 21273450]
55. Cheng C, Guo GF, Martinez JA, Singh V, Zochodne DW. Dynamic plasticity of axons within a cutaneous milieu. J Neurosci. 2010; 30(44):14735–14744. [PubMed: 21048132]
56. Koster MI. Making an epidermis. Ann N Y Acad Sci. 2009; 1170:7–10. [PubMed: 19686098]
57. Verze L, Viglietti-Panzica C, Maurizo S, Sica M, Panzica G. Distribution of GAP-43 nerve fibers in the skin of the adult human hand. Anat Rec A Discov Mol Cell Evol Biol. 2003; 272(1):467–473. [PubMed: 12704705]
58. Chhibber A, et al. Polygenic inheritance of paclitaxel-induced sensory peripheral neuropathy driven by axon outgrowth gene sets in CALGB 40101 (Alliance). Pharmacogenomics J. 2014; 14(4):336–342. [PubMed: 24513692]
59. Harrington AW, Ginty DD. Long-distance retrograde neurotrophic factor signalling in neurons. Nat Rev Neurosci. 2013; 14(3):177–187. [PubMed: 23422909]
60. Maday S, Wallace KE, Holzbaur EL. Autophagosomes initiate distally and mature during transport toward the cell soma in primary neurons. J Cell Biol. 2012; 196(4):407–417. [PubMed: 22331844]
61. Nie D, Sahin M. A genetic model to dissect the role of Tsc-mTORC1 in neuronal cultures. Methods Mol Biol. 2012; 821:393–405. [PubMed: 22125080]
62. Broeke JH, et al. Automated quantification of cellular traffic in living cells. J Neurosci Methods. 2009; 178(2):378–384. [PubMed: 19146878]
63. Nie D, et al. Tsc2-Rheb signaling regulates EphA-mediated axon guidance. Nat Neurosci. 2010; 13(2):163–172. [PubMed: 20062052]
64. Pekkurnaz G, Trinidad JC, Wang X, Kong D, Schwarz TL. Glucose regulates mitochondrial motility via Milton modification by O-GlcNAc transferase. Cell. 2014; 158(1):54–68. [PubMed: 24995978]
65. Pani G, et al. MorphoNeuroNet: an automated method for dense neurite network analysis. Cytometry A. 2014; 85(2):188–199. [PubMed: 24222510]

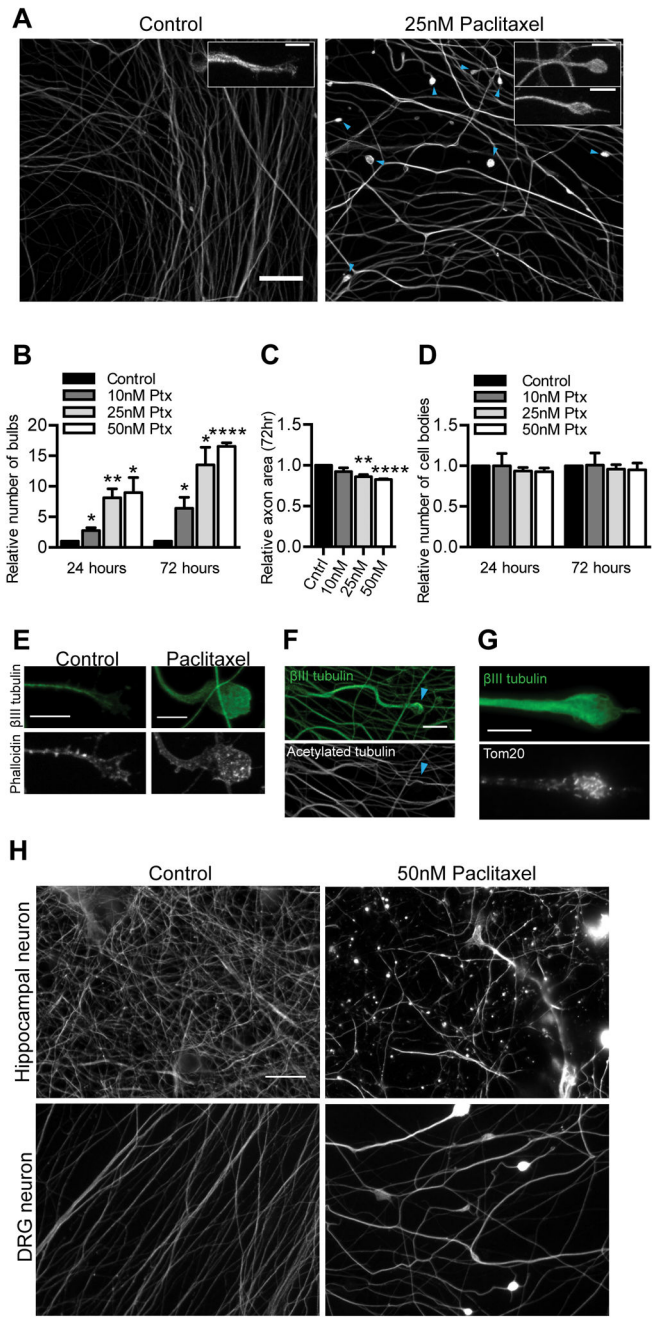

Fig 1. Effects of paclitaxel exposure on cultured adult DRG neurons

A) In DRG cultures immunostained for βIII tubulin, swellings (blue arrowheads) are present at axon tips after 25 nM paclitaxel treatment for 72 hr starting at 4 DIV, but not in control cultures. Scale bar, 20 μm. Insets compare a normal growth cone in control cultures and paclitaxel-induced retraction bulbs. Scale bars, 5 μm.

B–D) Quantification of DRG neurons treated with paclitaxel at the indicated concentrations for 24 or 72 hr, beginning at 4 DIV and stained for βIII tubulin. In each case, values for control cultures plated the same day were set as 1 and fold changes in response to paclitaxel treatment were calculated. n=3 experiments. (B) Number of retraction bulbs per field.

Relative to control, p=0.019 (10 nM), p=0.0078 (25 nM), p=0.033 (50 nM) at 24 hr, and p=0.038 (10 nM), p=0.012 (25 nM), p<0.0001 (50 nM) at 72 hr; Student's *t* test. (C) Axon area at 72 hr was calculated from masks created from original images. **p<0.01, ***p<0.001; Student's *t* test. (D) Number of cell bodies per field. p>0.05, Student's *t* test. E) A control growth cone and a paclitaxel-induced retraction bulb stained for F-actin with rhodamine-phalloidin and for βIII tubulin after three days of treatment. Scale bar, 5 μm. F–G) Paclitaxel-treated DRG neurons immunostained for βIII tubulin and acetylated tubulin (F) or the mitochondrial marker Tom20 (G) after three days of treatment. Retraction bulbs had no detectable acetylated tubulin but a concentration of mitochondria. Scale bars, 10 μm. H) Hippocampal neurons (7 DIV) and DRG neurons (4 DIV) were each treated with 50 nM paclitaxel for 3 days and then stained for βIII tubulin. Paclitaxel induced greater degeneration in hippocampal neurons Scale bar, 20 μm.
Ptx, paclitaxel.

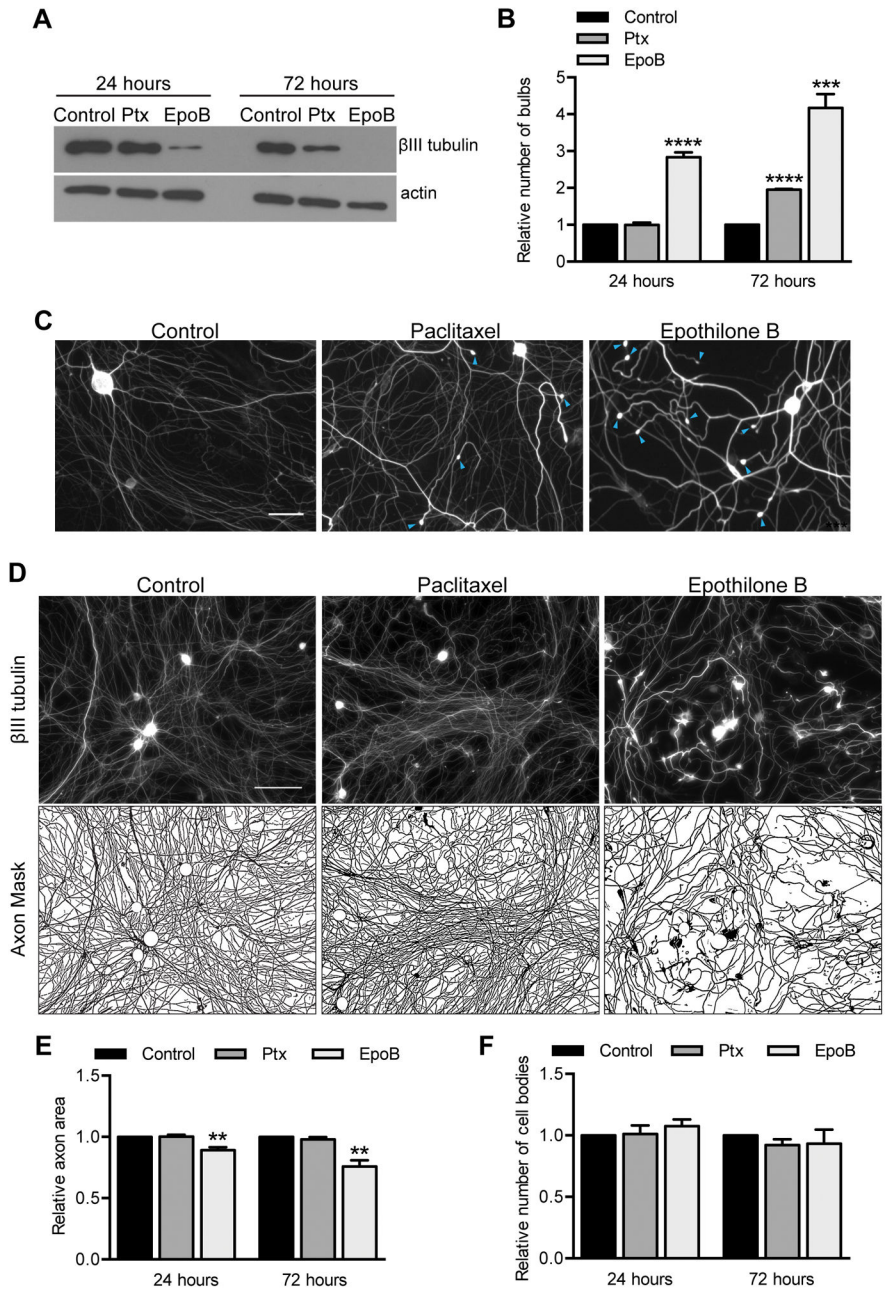

Fig 2. The neurotoxicity of epothilone B and paclitaxel correlates with their microtubule stabilization

Cultured DRG neurons were treated with 2 nM paclitaxel or epothilone B starting at 3 DIV and treatment was refreshed every 8 hr for 24 or 72 hr.

A) After epothilone B treatment, lower levels of soluble tubulin remained than after paclitaxel due to the greater potency of epothilone at stabilizing polymerized tubulin. Actin serves as a loading control.

B) Quantification of retraction bulbs per field. The number of retraction bulbs in control cultures was set as 1 and fold changes in response to paclitaxel and epothilone B treatment were calculated. ***p<0.001, ****p<0.0001; Student's *t* test.

C) Representative fields immunostained for βIII tubulin with retraction bulbs (blue arrowheads) at 72 hr, as quantified in (B). Scale bar, 50 μm.
D–E) To assess axon area after 72 hr of treatment, cell bodies were removed from the images and an axon mask was created. Axon area was then quantified and expressed as fold change compared control. Scale bar, 100 μm. **p<0.01, Student's *t* test.
F) The number of cell bodies per field was counted from images like those in (D) and expressed as fold change compared to control. p>0.05, Student's *t* test.
For (A–F), n=4 experiments. Ptx, paclitaxel.

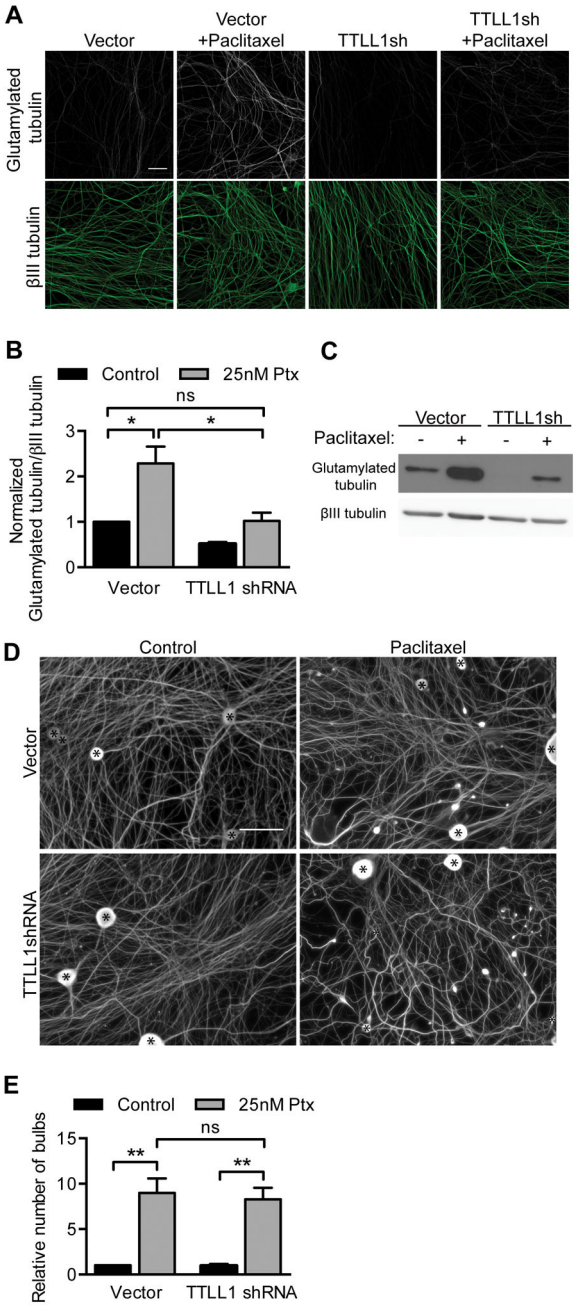

Fig 3. Maintaining control levels of glutamylated tubulin after paclitaxel treatment does not rescue paclitaxel neurotoxicity

A–B) DRG cultures were infected with TTLL1 shRNA lentivirus or control vector at 0 DIV, treated for 24 hr with 25 nM paclitaxel at 6 DIV, and immunostained for βIII tubulin and glutamylated tubulin. The fluorescence intensity of glutamylated tubulin signal from axons was normalized to βIII tubulin signal, and fold changes relative to control were calculated. Scale bar, 20 μm. p=0.026 (Vector vs. Vector 25 nM), p=0.037 (Vector 25 nM vs. TTLLsh 25 nM), ns p=0.92; Student's *t* test.

C) Glutamylated tubulin and βIII tubulin in Western blots of lysates of DRG cultures as in (A). TTLL1 shRNA reduced tubulin glutamylation in the presence of paclitaxel to control levels.

D–E) DRG cultures as in (A) and immunostained for βIII tubulin show retraction bulbs after paclitaxel treatment whether or not glutamylation was inhibited. Cell bodies are indicated by asterisks (*). Number of retraction bulbs per field is expressed as a fold change relative to control. Scale bar, 50 μm. **p<0.01, ns p=0.75; Student's *t* test.

For (A–E), n=3 experiments. Ptx, paclitaxel.

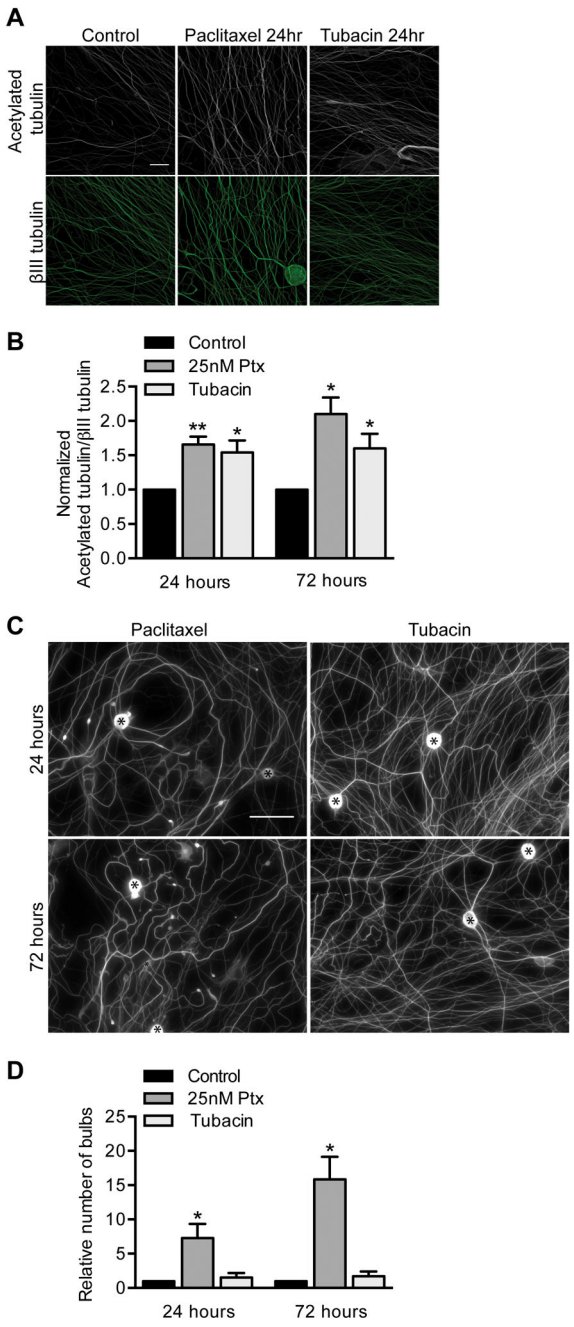

Fig 4. Increasing acetylated tubulin with tubacin does not mimic paclitaxel neurotoxicity

DRG neurons at 3 DIV were treated with 20 μM tubacin or 25 nM paclitaxel for 24 or 72 hr refreshed every 24 hr.

A–B) The immunofluorescence intensity of acetylated tubulin in axons was normalized to the βIII tubulin immunofluorescence, and fold changes from control were calculated. Scale bar, 20 μm. Relative to control, p=0.0049 (25 nM Ptx), p=0.036 (tubacin) at 24 hr, and p=0.010 (25 nM Ptx), p=0.047 (tubacin) at 72 hr; Student's *t* test.

C–D) 25 nM paclitaxel but not 20 μM tubacin treatment caused retraction bulbs to form as visualized with anti-βIII tubulin (C) and quantified per field (D). Scale bar, 50 μm. Cell

bodies are indicated by asterisks (*). Relative to control, p=0.038 (25 nM Ptx), p=0.46 (tubacin) at 24 hr, and p=0.011 (25 nM Ptx), p=0.35 (tubacin) at 72 hr; Student's *t* test. For (A–D), n=3 experiments. Ptx, paclitaxel.

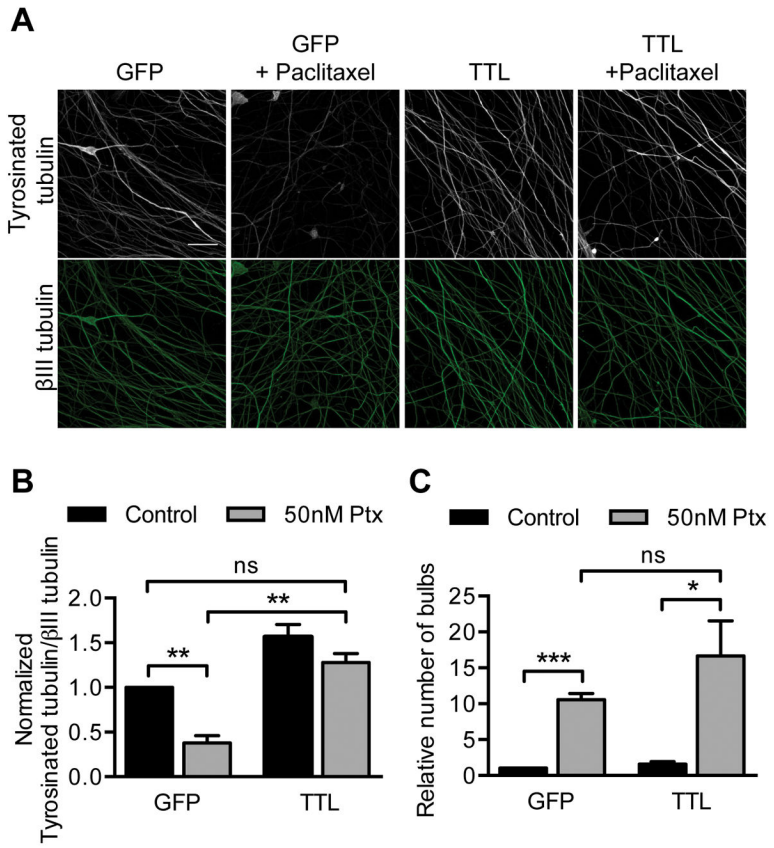

Fig 5. Maintaining control levels of tyrosinated tubulin after paclitaxel treatment does not rescue paclitaxel neurotoxicity

TTL or GFP control lentivirus was added to DRG neurons at 0 DIV and treated with 50 nM paclitaxel for 48 hr starting at 5 DIV prior to immunostaining for tyrosinated tubulin and βIII tubulin at 7 DIV.

A–B) The fluorescence intensity of tyrosinated tubulin signal from axons was normalized to βIII tubulin signal, and fold changes from control were calculated. Scale bar, 20 μm. **p<0.01, ns p=0.18; Student's *t* test.

C) Number of retraction bulbs per field was quantified and is expressed as a fold change relative to control. ***p<0.001, *p=0.037, ns p=0.28; Student's *t* test.

For (A–C) n= 3 experiments. Ptx, paclitaxel.

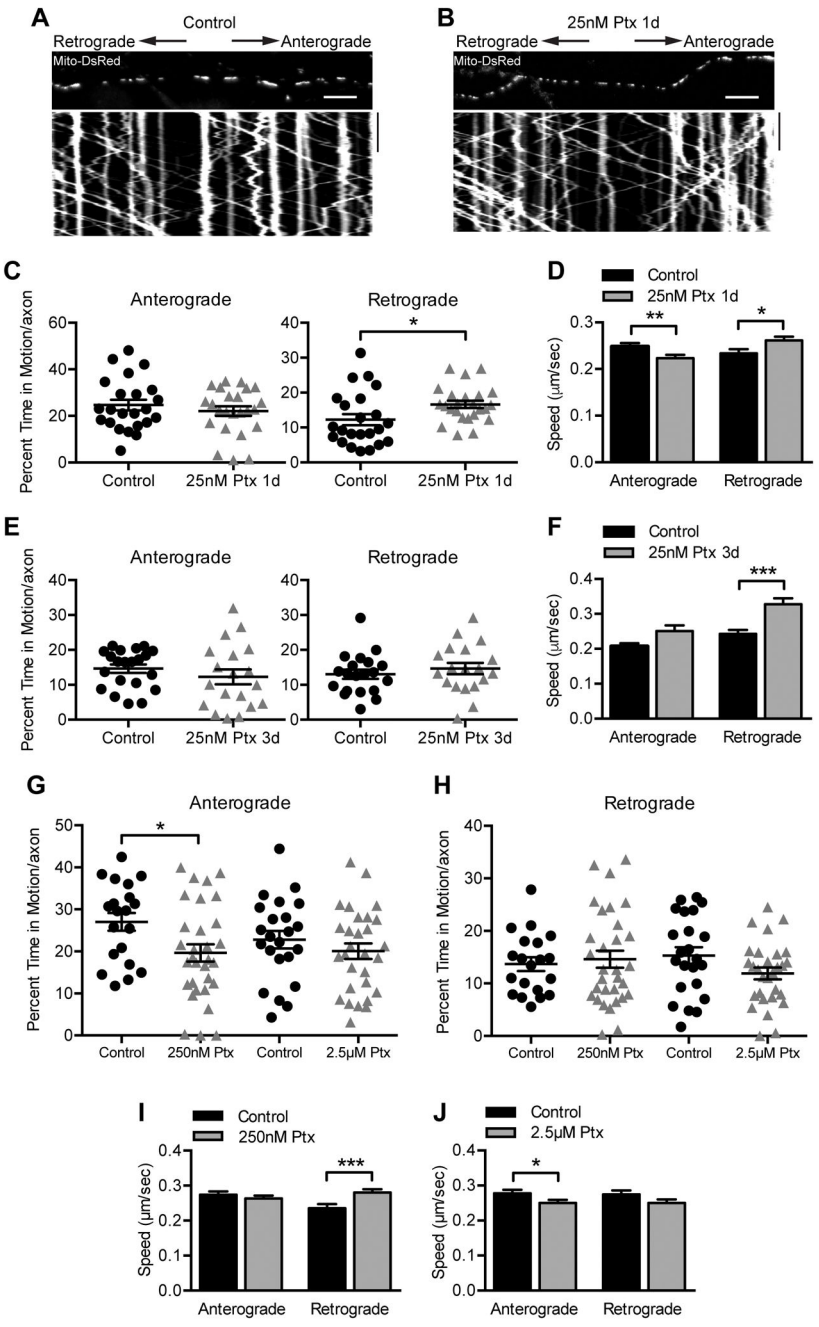

Fig 6. Axonal transport of mitochondria persists after paclitaxel exposure

A–B) Kymographs of mitochondrial movement in DRG axons infected with Mito-DsRed lentivirus and treated with DMSO as a control (A) or 25 nM paclitaxel (B) for 1 day prior to imaging at 4 DIV. Kymographs represent position (x axis) over time (y axis) such that vertical lines indicate stationary mitochondria and diagonal lines indicate moving mitochondria. The image above the kymograph is the first frame of the time lapse movie used to generate the kymograph. Scale bars, 10 μm 100 s.

C) The percent of time that mitochondria moved in either the anterograde or retrograde direction per axon after treatment with DMSO control or 25 nM paclitaxel for 1 day was

quantified using kymographs like those in (A) and (B). n=23–24 axons from 4 independent experiments. *p=0.026, Student's *t* test.

D) The average speed of each mitochondrion moving either anterograde or retrograde after treatment with DMSO control or 25 nM paclitaxel for 1 day was quantified using kymographs like those in (A) and (B). n=371–410 (anterograde) and n=222–322 (retrograde) mitochondria from 4 experiments. *p=0.029, **p<0.01; Mann-Whitney *U* test.

E) Quantification of the percent of time mitochondria were moving after treatment with DMSO control or 25 nM paclitaxel for 3 days, replenished every 24 hr. n=19–21 axons from 4 experiments. p>0.05, Student's *t* test.

F) Quantification of the average speed of each mitochondrion after treatment with DMSO control or 25 nM paclitaxel for 3 days, replenished every 24 hr. n=191–214 (anterograde) and 195–212 (retrograde) mitochondria from 4 experiments. ***p<0.001, Mann-Whitney *U* test.

G–J) Quantification of mitochondrial parameters as in (C–F), but in the presence of higher paclitaxel concentrations for 6–9 hr. (G–H) n=20–31 axons from 5 experiments. *p=0.02, Student's *t* test. (I) n=241–309 (anterograde) and n=160–256 (retrograde) mitochondria from 5 experiments. ***p<0.001, Mann-Whitney *U* test. (J) n=246–292 (anterograde) and n=198–207 (retrograde) mitochondria from 5 experiments. *p=0.047, Mann-Whitney *U* test.

Ptx, paclitaxel.

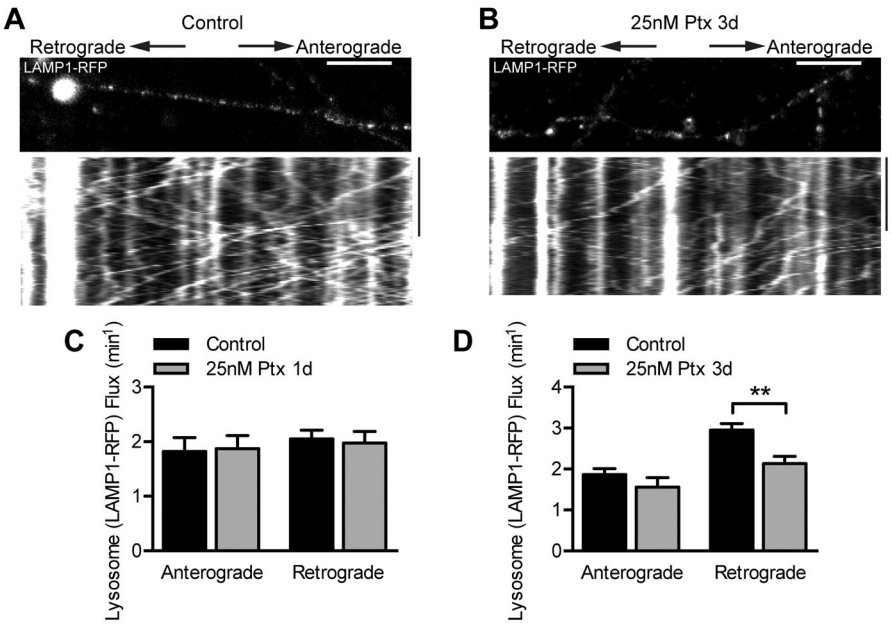

Fig 7. Effect of paclitaxel on lysosome transport

A–B) Kymographs of lysosome movement in DRG axons infected with LAMP1-RFP lentivirus and treated with DMSO as a control (A) or 25 nM paclitaxel (B) for 3 days, and imaged at 6 DIV. The image above the kymograph is the first frame of the time lapse movie used to generate the kymograph. Scale bars, 10 μm 100 s.

C–D) Average anterograde and retrograde lysosome flux per axon after treatment with DMSO control or 25 nM paclitaxel for 1 day (C) or 3 days (D). Flux was quantified from kymographs like those in (A) and (B) by counting LAMP1-RFP tracks that crossed a line drawn in the center of the kymograph. n=17–19 axons from 3 experiments. **p<0.01, Student's *t* test.

Ptx, paclitaxel.

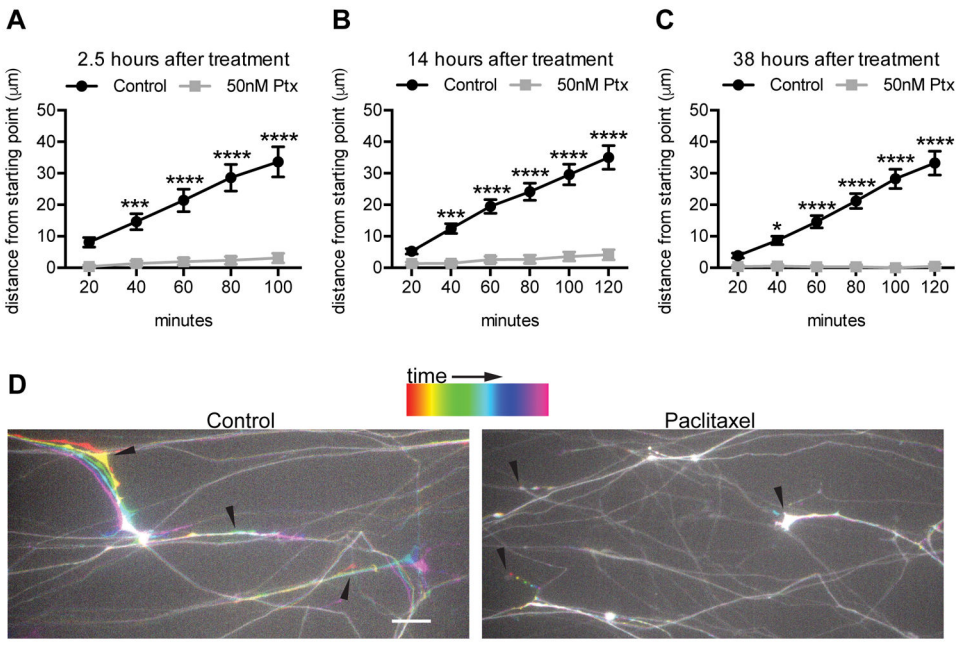

Fig 8. Paclitaxel quickly and stably inhibits DRG axon growth

DRG neurons infected with GFP lentivirus at DIV 0 were grown 6 days in culture and then treated with 50 nM paclitaxel. Images of the same fields of GFP+ distal axons were taken every 20 min for 100–120 min at 2.5 hr, 14 hr, and 38 hr after paclitaxel or DMSO control treatment.

A–C) The distance in microns that each axon ending moved (grew or retracted) relative to t=0 was measured for each time interval. n=41–50 axons from 2 experiments.

D) Temporal color coding of the 100 min time lapse beginning 2.5 hr after paclitaxel addition. Arrowheads indicate the starting points of the indicated axon endings. While axon growth occurred in the control treatment, little to no growth or retraction was seen after paclitaxel treatment. Scale bar, 20 μm.

*p<0.05, ***p<0.001, ****p<0.0001; two-way ANOVA with Bonferroni correction. Ptx, paclitaxel.

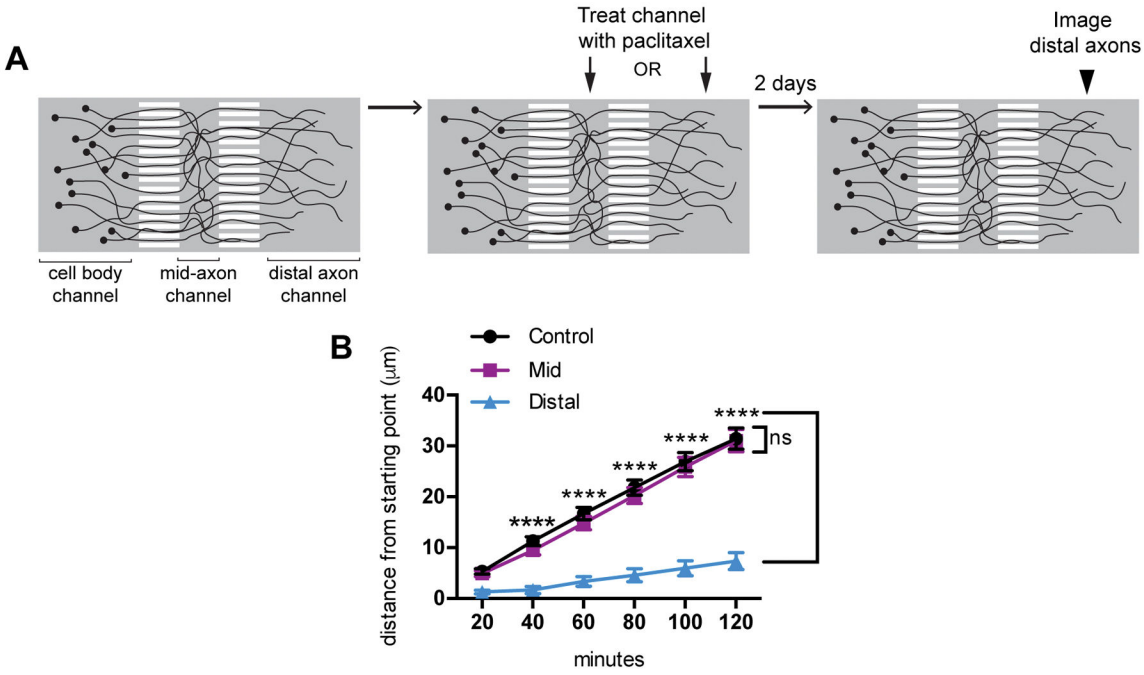

Fig 9. Paclitaxel exposure of the distal axon, but not the mid-axon, disrupts axon outgrowth

A) Schematic of the use of microfluidic devices to examine the effects of exposing either the distal portion of the axon or a mid-axonal segment to paclitaxel. The culture chamber consists of 3 fluidically isolated compartments (cell body, mid-axon and distal axon) connected by 2 sets of microgrooves. Starting at 6 DIV, either the mid-axon or distal axons were exposed to 50 nM paclitaxel for two days after which distal axons were imaged every 20 min for 120 min.

B) The distance in microns that each axon ending moved (grew or retracted) relative to t=0 was measured for each experimental condition. n= 252–308 axons from 4–5 experiments per condition.

****$p<0.0001$, ns $p>0.05$; two-way ANOVA, Dunnett's post test. Ptx, paclitaxel.